BULLETIN OF THE EARTHQUAKE
RESEARCH INSTITUTE
Vol. 47 (1969), pp. 875-890

40. A Long Wave around a Breakwater [VIII].

—Case of Oblique Incidence—

By Takao MOMOI,

Earthquake Research Institute.

(Read May 27, 1969.—Received July 30, 1969.)

Abstract

The long wave around the breakwater gap is discussed for the case of the oblique incidence of a train of periodic waves. In the analysis, the incident wave always meets at a sharp angle with the right-hand breakwater. The most conspicuous features found in the analysis are as follows. A reverse current appears in the windward waters around the terminus of the left-hand breakwater for the wave of long wavelength which is the current against the direction of the incident wave travel. The stagnation point discriminating between the above reverse current and the advancing one is in a sense moving away from the breakwater gap along the left-hand breakwater for the increase of the incident angle of the incoming wave. In the analysis concerning the influence of the breakwater wing upon the diffracted wave from the other breakwater, it is found that the wave is reflected from the breakwater shadow.

1. Introduction

Succeeding the previous works (*Momoi*, 1967a-1969b), the long wave around the breakwater gap is discussed in this paper for the case of the oblique incidence of a train of periodic waves. The basic method is the method of the buffer domain which was outlined in Section *2*, *3* of the first paper (*Momoi*, 1967a). The points of discussion are the wave behaviors due to the oblique incidence of the incident wave.

2. Theory

2,1. Geometry of the Model Used.

The breakwaters are assumed to be thin plates of infinitesimal thickness, which run along a single straight line with a small gap to separate the infinitely extending waters of uniform depth (H) into two semi-infinite ones. The coordinate is centered, referring to Fig. 1, at the

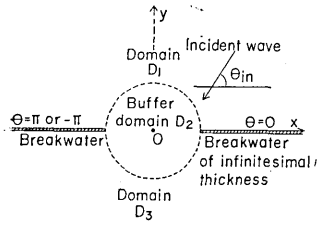

Fig. 1. Geometry of the model used.

undisturbed water surface of the midpoint of the breakwater gap, the breadth of which is $2d$, the breakwaters being situated on the x-axis of the cartesian coordinate with the positive direction of the y-axis on the windward side. A train of periodic plane waves is then propagated toward the breakwater wings with the inclination of θ_{in} radians, which is stated by

$$\left.\begin{aligned} \phi_{in}&=\phi_0 \exp(-i\omega t-ik_1x-ik_2y)\cosh k(z+H),\\ k_1&=k\cos\theta_{in}, \qquad k_2=k\sin\theta_{in}, \end{aligned}\right\} \tag{1}$$

where

ϕ_{in} : the velocity potential of the incident wave,
ϕ_0 : the amplitude of the velocity potential of the incident wave,
ω : the angular frequency of the incident wave,
k : the wave number of the incident wave,
t : the time variable,
z : the z-component of the cartesian coordinate with the positive upward.

In the above expression, only the real part has a physical meaning.

2,2. Basic Equation and Boundary Conditions.

Assuming irrotational and infinitesimal motion in incompressible fluid. the velocity potential satisfies the equation

$$\left(\frac{\partial^2}{\partial x^2}+\frac{\partial^2}{\partial y^2}+\frac{\partial^2}{\partial z^2}\right)\phi=0\,. \tag{2}$$

Let ζ and g be, respectively, the elevation of water surface and the gravity constant. ζ is expressed as (the relation of energy)

$$\zeta=\frac{1}{g}\left(\frac{\partial\phi}{\partial t}\right)_{z=0}. \tag{3}$$

On the other hand, we have, as a kinematical condition,

$$\frac{\partial\zeta}{\partial t}=-\left(\frac{\partial\phi}{\partial z}\right)_{z=0}. \tag{4}$$

Equations (3) and (4) are the conditions at the surface of water.

As the condition at the bottom, we have

$$\frac{\partial \phi}{\partial z}=0 \qquad \text{at} \quad z=-H\,. \tag{5}$$

The conditions at the rigid wall of the breakwater is

$$\frac{\partial \phi}{\partial y}=0 \qquad \text{at} \quad y=0,\ |x|>d\,. \tag{6}$$

2,3. Formal Solution.

In our model, the entire domain is, referring to Fig. 1, separated into three parts, i.e.,

domain D_1: the region in the range $0<\theta<\pi$ and $d<r$ (non-buffer domain),

domain D_2: the region in the range $r<d$ (buffer domain),

domain D_3: the region in the range $-\pi<\theta<0$ and $d<r$ (non-buffer domain),

where r and θ are the radial and azimuthal components of the polar coordinate.

The formal expessions are then described as follows.

$$\phi_{xy}^{(1)}=\phi_0 \exp(-ik_1x-ik_2y)+\phi_0(-ik_1x+ik_2y) + \sum_{m=0}^{\infty}\phi_1^{(m)}H_m^{(1)}(kr)\cos m\theta \tag{7}$$

in domain D_1,

$$\phi_{xy}^{(2)}=\sum_{m=0}^{\infty}(\bar{\phi}_2^{(m)}\cos m\theta+\phi_2^{(m)}\sin m\theta)J_m(kr) \tag{8}$$

in domain D_2,

$$\phi_{xy}^{(3)}=\sum_{m=0}^{\infty}\phi_3^{(m)}H_m^{(1)}(kr)\cos m\theta \tag{9}$$

in demain D_3,

where $\phi_{xy}^{(j)}$ $(j=1, 2, 3)$ denote the horizontal factors of the velocity potentials ϕ_j $(j=1, 2, 3)$ in domain D_j $(j=1, 2, 3)$, which are related by

$$\phi_j=\phi_{xy}^{(j)}\cosh k(z+H) \quad (j=1, 2, 3)\,, \tag{10}$$

and where $\phi_1^{(m)}$, $\bar{\phi}_2^{(m)}$, $\phi_2^{(m)}$, $\phi_3^{(m)}$ are the unknown factors to be determined by the boundary conditions between the adjacent domains. Expression (10) satisfies the conditions (3) to (6).

2,4. Condition between Adjacent Domains.

Since the depth of the waters is assumed to be uniform through the entire domain, the conditions between the adjacent domains are described by use of only horizontal factors $\phi_{xy}^{(j)}$ $(j=1, 2, 3)$ of the velocity potentials

as follows.

$$\left.\begin{aligned} \phi_{xy}^{(2)} &= \phi_{xy}^{(1)} \\ \frac{\partial\phi_{xy}^{(2)}}{\partial r} &= \frac{\partial\phi_{xy}^{(1)}}{\partial r} \end{aligned}\right\} (r=d,\ 0<\theta<\pi) \qquad \left.\begin{aligned} \phi_{xy}^{(2)} &= \phi_{xy}^{(3)} \\ \frac{\partial\phi_{xy}^{(2)}}{\partial r} &= \frac{\partial\phi_{xy}^{(3)}}{\partial r} \end{aligned}\right\} (r=d,\ \pi<\theta<2\pi)\ . \tag{11}$$

2,5. Infinite Simultaneous Equations.

Using formal expressions (7) to (9) and conditions (11), the following simultaneous equations are obtained.

$$\frac{2}{\pi}\varepsilon_n \sum_{m=0}^{\infty} \phi_2^{(2m+1)} \frac{2m+1}{(2m+1)^2-(2n)^2} \begin{Bmatrix} J_{2m+1}(kd) \\ J'_{2m+1}(kd) \end{Bmatrix} - \phi_1^{(2n)} \begin{Bmatrix} H_{2n}^{(1)}(kd) \\ H_{2n}^{(1)\prime}(kd) \end{Bmatrix} = \phi_0 \varepsilon_n (-1)^n \cos 2n\theta_{in} \begin{Bmatrix} J_{2n}(kd) \\ J'_{2n}(kd) \end{Bmatrix} \tag{12}$$

$$(\varepsilon_0=1,\ \varepsilon_n=2 \text{ for } n\geqq 1,\ n=0, 1, 2, \cdots)\ ,$$

$$\frac{4}{\pi} \sum_{m=1}^{\infty} \phi_2^{(2m)} \frac{2m}{(2m)^2-(2n+1)^2} \begin{Bmatrix} J_{2m}(kd) \\ J'_{2m}(kd) \end{Bmatrix} - \phi_1^{(2n+1)} \begin{Bmatrix} H_{2n+1}^{(1)}(kd) \\ H_{2n+1}^{(1)\prime}(kd) \end{Bmatrix} = i\phi_0 2(-1)^{n+1} \cos (2n+1)\theta_{in} \begin{Bmatrix} J_{2n+1}(kd) \\ J'_{2n+1}(kd) \end{Bmatrix} \tag{13}$$

$$(n=0, 1, 2, \cdots)\ .$$

The reductions made in the above go along the same lines as those in Section *2,5* of the fourth work (*Momoi*, 1968b). The above equations refer to those of (33) and (34) in the fourth work.

In the course of the above reductions, the relations

$$\left.\begin{aligned} \bar{\phi}_2^{(2n)} &= \phi_0 \varepsilon_n (-1)^n \cos 2n\theta_{in}\ , \\ \bar{\phi}_2^{(2n+1)} &= i\phi_0 2(-1)^{n+1} \cos (2n+1)\theta_{in}, \\ \phi_1^{(n)} &= -\phi_3^{(n)}\ , \end{aligned}\right\} (n=0, 1, 2, \cdots) \tag{14}$$

are derived.

Elimination of $\phi_1^{(2n)}$ and $\phi_1^{(2n+1)}$, respectively, from equations (12) and (13) yields

$$\sum_{m=0}^{\infty} \phi_2^{(2m+1)} \frac{2m+1}{(2m+1)^2-(2n)^2} \{J_{2m+1}(kd) H_{2n}^{(1)\prime}(kd) - J'_{2m+1}(kd) H_{2n}^{(1)}(kd)\} = i\phi_0 (-1)^n \cos 2n\theta_{in}/kd\ , \tag{15}$$

$$\sum_{m=1}^{\infty}\phi_2^{(2m)}\frac{2m}{(2m)^2-(2n+1)^2}\{J_{2m}(kd)H_{2n+1}^{(1)\prime}(kd)-J_{2m}'(kd)H_{2n+1}^{(1)}(kd)\}$$
$$=\phi_0(-1)^n\cos(2n+1)\theta_{in}/kd\ , \tag{16}$$

where $n=0, 1, 2, \cdots$.

2,6. Simplified Forms of Formal Solution.

Substituting (14) into formal expressions (7) to (9), these are reduced to the following.

$$\left.\begin{aligned}
\phi_{xy}^{(1)}&=\phi_0\exp(-ik_1x-ik_2y)+\phi_0\exp(-ik_1x+ik_2y)\\
&\quad+\phi_{sc}^{(1)}(r,\theta_1)\qquad(0<\theta_1<\pi)\ ,\\
\phi_{xy}^{(2)}&=\frac{1}{2}\phi_0\exp(-ik_1x-ik_2y)+\frac{1}{2}\phi_0\exp(-ik_1x+ik_2y)\\
&\quad+\sum_{m=1}^{\infty}\phi_2^{(m)}J_m(kr)\sin m\theta\qquad(0\leqq\theta<2\pi)\ ,\\
\phi_{xy}^{(3)}(r,\theta_3)&=-\phi_{xy}^{(1)}(r,\theta_1)\qquad(\theta_3=-\theta_1)\ ,
\end{aligned}\right\} \tag{17}$$

where

$$\phi_{sc}^{(1)}(r,\theta_1)=\sum_{m=0}^{\infty}\phi_1^{(m)}H_m^{(1)}(kr)\cos m\theta_1\ . \tag{18}$$

In the above derivation, the reduction

$$\exp(-ik_1x\mp ik_2y)=\exp\{-ikr\cos(\theta\mp\theta_{in})\}$$
$$=\sum_{n=0}^{\infty}\varepsilon_n(-1)^nJ_{2n}(kr)\cos 2n(\theta\mp\theta_{in})$$
$$-i\sum_{n=0}^{\infty}2(-1)^nJ_{2n+1}(kr)\cos(2n+1)(\theta\mp\theta_{in})$$

is employed, where the double sign $\mp$ must be taken in the same order.

2,7. The $(2l+1)$th Approximation.

As the second step, the approximation is given to the expression of the buffer domain. That is to say, setting

$$\left.\begin{aligned}
J_m(kr)&\equiv 0\quad(m>2l+1)\\
J_m(kr)&\not\equiv 0\quad(m\leqq 2l+1)
\end{aligned}\right\}\qquad(l=1, 2, 3, \cdots) \tag{19}$$

for $r\leqq d$ in (17), the upper limit of $\sum$ of this equation becomes $2l+1$. Equations (15) and (16) are then reduced to the following.

$$\sum_{m=0}^{l} X_{2m+1} \frac{2m+1}{(2m+1)^2-(2n)^2} \left\{1-\frac{J'_{2m+1}(kd)H^{(1)}_{2n}(kd)}{J_{2m+1}(kd)H^{(1)\prime}_{2n}(kd)}\right\}$$
$$=i\phi_0(-1)^n \cos 2n\theta_{in}/\{kdH^{(1)\prime}_{2n}(kd)\} \tag{20}$$

and

$$\sum_{m=1}^{l} X_{2m} \frac{2m}{(2m)^2-(2n+1)^2} \left\{1-\frac{J'_{2m}(kd)H^{(1)}_{2n+1}(kd)}{J_{2m}(kd)H^{(1)\prime}_{2n+1}(kd)}\right\}$$
$$=\phi_0(-1)^n \cos (2n+1)\theta_{in}/\{kdH^{(1)\prime}_{2n+1}(kd)\}\ , \tag{21}$$

where $X_p=\phi_2^{(p)}J_p(kd)$ $(p=1, 2, \cdots, 2l+1)$ and $n=0, 1, 2, \cdots l$ $(l-1$ for (21)). It must here be noted that the quantities in the wavy bracket are normalized by $J_{2m+1}(kd)H^{(1)\prime}_{2n}(kd)$ in (20) and $J_{2m}(kd)H^{(1)\prime}_{2n+1}(kd)$ in (21). This procedure is preferable to avoid the truncation errors in the calculation of simultaneous equations. Using equations (20) and (21), the unknown factors

$$\phi_2^{(p)} \quad (p=1, 2, \cdots, 2l+1) \tag{22}$$

can be obtained.

As for the unknown factors $\phi_1^{(p)}$ in domain D_1, equations (12) and (13) are used. Substitution of (22) into the first equations of (12) and (13) yields

$$\phi_1^{(p)} \quad (p=0, 1, 2, \cdots)\ . \tag{23}$$

In using (12) and (13), the approximation (19) is taken into account for the calculation of Bessel and Hankel functions.

The unknown factors

$$\phi_3^{(p)} \quad (p=0, 1, 2, \cdots) \tag{24}$$

in domain D_3 are obtained from (23) and the last equation of (14).

Using the factors obtained in such a way, the wave around the breakwater gap can be discussed through formal expressions (17) to (18). The actual calculation of the above procedure is made with the aid of an electronic computer.

Since the depth of water is uniform, the relation between ζ and ϕ is given by

$$\zeta/\zeta_0=\phi/\phi_0 \tag{25}$$

where ζ_0 is the amplitude of the incident wave which is assumed as 1.0 in the following.

3. Computed Results

Following the afore-mentioned procedures, numerical calculations are carried out.

3,1. Validity of Our Theory.

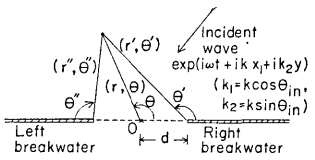

Fig. 2. Nomenclature of the model used.

To begin with, the validity of our theory is verified through the use of an approximated theory based on Stoker's solution around a *single* breakwater wing (*Stoker*, 1957). The approximated theory is described in the following.

$$\zeta_{ap}=\zeta_{right}+\zeta_{left}-\exp(ik_1x+ik_2y)\ , \quad (26)$$

where

$$\left.\begin{aligned}&\zeta_{right}=\exp(ik_1d)\cdot f(kr',\theta',\theta_{in})\ ,\\&\zeta_{left}=\exp(-ik_1d)\cdot f(kr'',\theta'',\pi-\theta_{in})\ ,\\&f(\rho,\theta,\varphi)=J_0(\rho)+2\sum_{n=1}^{\infty}\exp\left(\frac{in\pi}{4}\right)J_{n/2}(\rho)\cdot\cos\left(\frac{n\varphi}{2}\right)\cos\left(\frac{n\theta}{2}\right).\end{aligned}\right\} \quad (27)$$

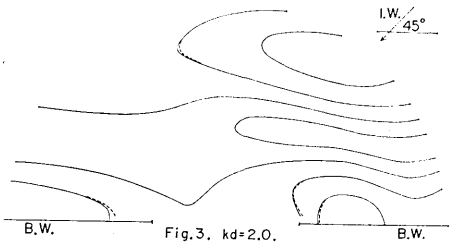

Fig.3. kd=2.0.

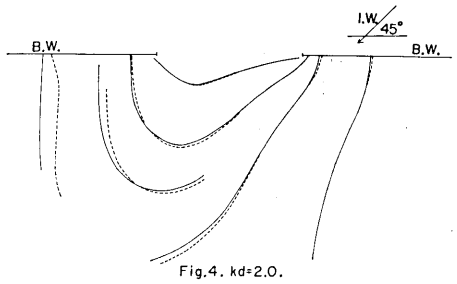

Fig.4. kd=2.0.

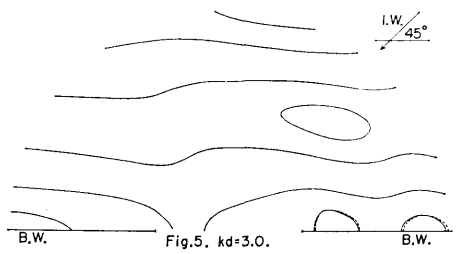

Fig.5. kd=3.0.

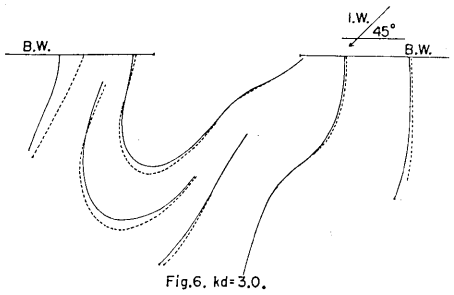

Fig.6. kd=3.0.

Figs. 3-6. Comparison of two results calculated on the basis of the method of the buffer domain and the approximated method.*

* **I. W.** and **B. W.** are the abbreviations of "incident wave" and "breakwater".

For the definitions and notations, Fig. 2 should be referred to. As be readily found from expression (26), only the primary reflection at the breakwater has been allowed for. Since the secondary reflection continues weakening with the increase of kd, the above approximated theory might be well expressible of the real phenomena of the wave around the breakwater gap. Using expression (26) and the procedure described in a previous section, the conformity of two theories are examined for the incident angle of $\theta_{in}=45$ degrees. The result is given in Figs. 3 to 6, in which the curves depicted by $|\zeta|$ (given by (25)) and $|\zeta_{ap}|$ (given by (26)) are, respectively, the solid and broken lines. These figures show a good agreement of the two theories. Our theory based on the method of the buffer domain developed in the foregoing section is therefore well applicable to the present problem.

3,2. RST Wave.

The RST wave is the abbreviation of resultant wave, which is expressed by (25) through the use of (17) to (18). The calculations are based on $|\bar{\zeta}_{rst}|$ for the amplitude and arg $\bar{\zeta}_{rst}$ for the phase*, where $\bar{\zeta}_{rst}$ is the conjugate value of the wave height of the RST wave.

To begin with, the calculation is carried out for a specified value $\theta_{in}=45$ degrees ($=\pi/4$ radians) in the range $kd=0.01$ to 3.0. The results are presented in Figs. 7aw to 12aw for the amplitude in the windward waters, Figs. 7pw to 12pw for the phase in the windward waters, Figs. 7al to 12al for the amplitude in the leeward waters and Figs. 7pl to 12pl for the phase in the leeward waters. Inspection of Figs. 7aw to 12aw shows that the contours of the amplitude run in a circular from around the breakwater gap for small kd (the case of Figs. 7aw and 8aw) and that the high waves (>2.0 in amplitude) appear along the breakwater and in the offing with the increase of kd which are characterized by the shadow (the case of Figs. 9aw to 12aw). As for the phase variation in the windward waters (Figs. 7pw to 12pw), the most conspicuous feature is an appearance of *reverse current* in the nearby waters of the leeward (left-hand) breakwater for small kd (refer to Figs. 7pw to 9pw). For the generation of the reverse current, the same phenomenon has already been found in the fourth work (*Momoi*, 1968b) with lateral incidence of the incident wave. In the leeward waters, the contours of the amplitude and phase are almost in a circular shape for kd in the range 0.01 to 0.1 (the case of Figs. 7al(pl) and 8al(pl)). As kd increases, the directivity of the wave continues growing, which are

* The degree of the employed approximation is taken highly enough to keep good convergence for the calculated results.

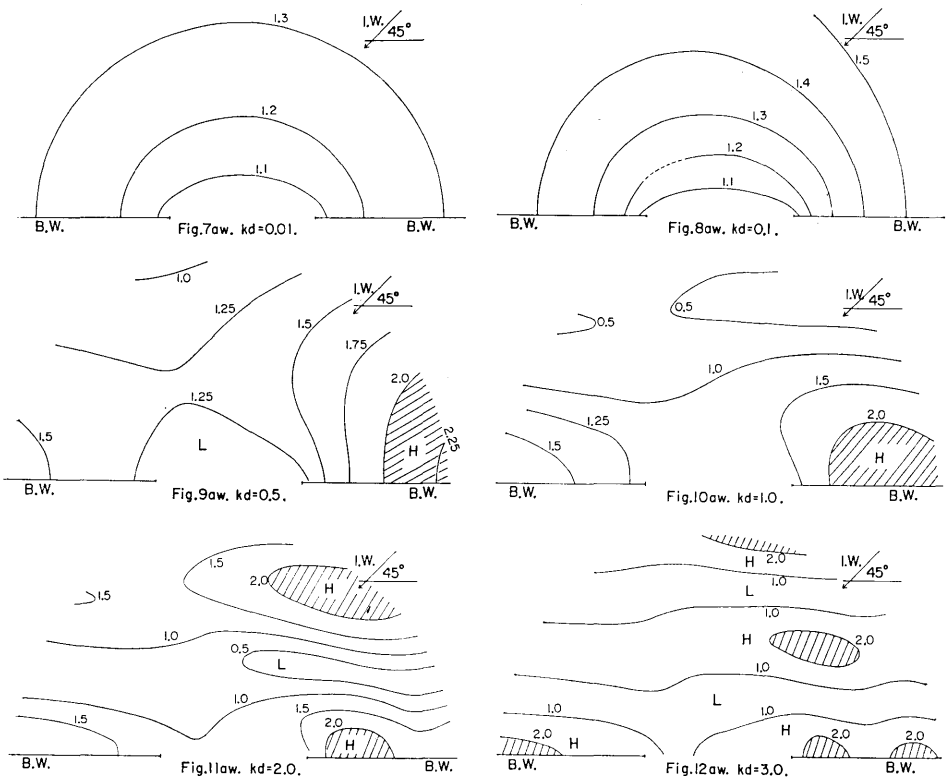

Figs. 7aw–12aw. Amplitude variation of RST wave in the windward waters.*

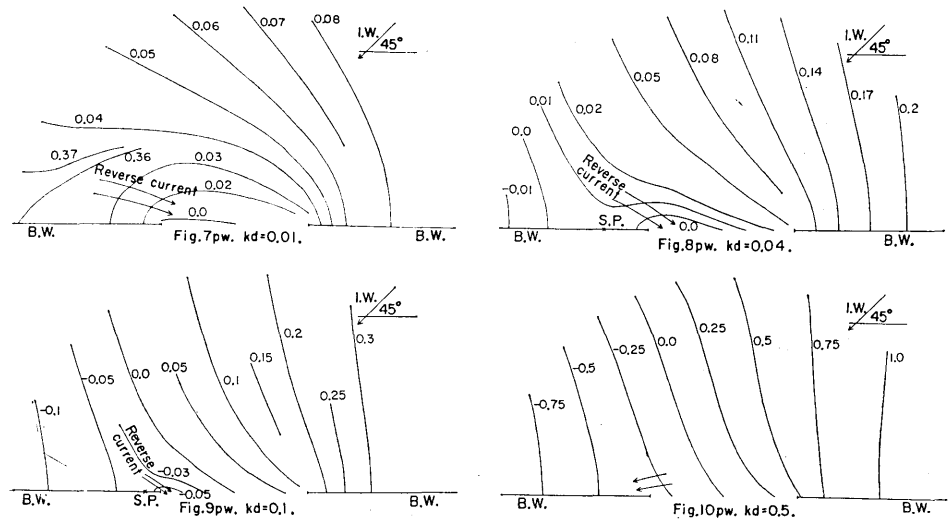

(to be continued)

* See the footnote of Figs. 3-6.

(continued)

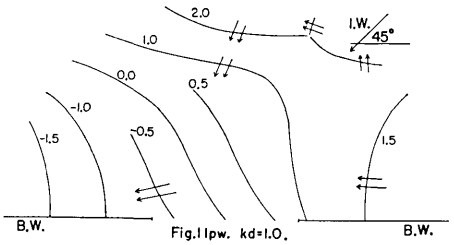

Fig.11pw. kd=1.0.

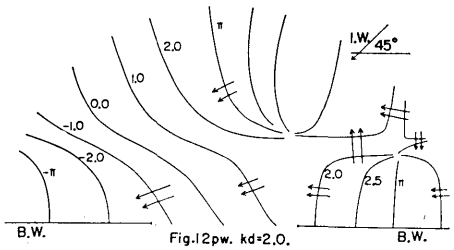

Fig.12pw. kd=2.0.

Figs. 7pw–12pw. Phase variation of RST wave in the windward waters.* **S. P.** is the separating point between the advancing and the reverse currents.

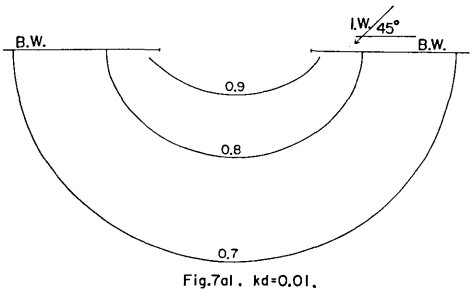

Fig.7al. kd=0.01.

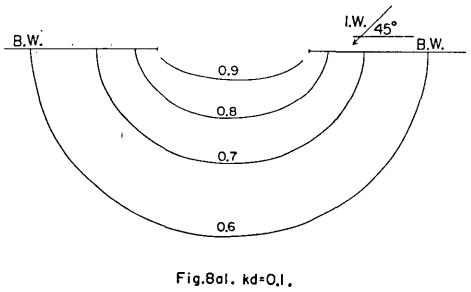

Fig.8al. kd=0.1.

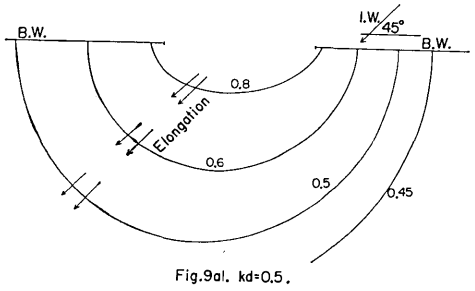

Fig.9al. kd=0.5.

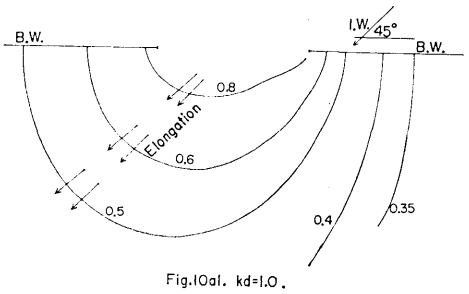

Fig.10al. kd=1.0.

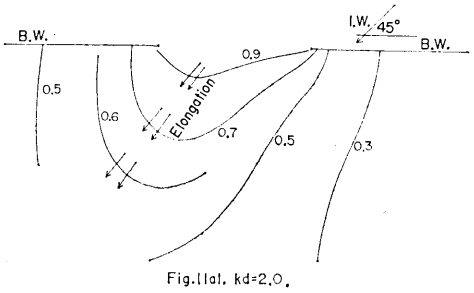

Fig.11al. kd=2.0.

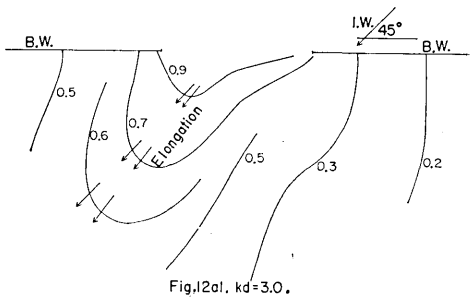

Fig.12al. kd=3.0.

Figs. 7al–12al. Amplitude variation of RST wave in the leeward waters.* Note the gradual elongation of the contours showing the increasing sense of the directivity of the wave.

* See the footnote of Figs. 3–6.

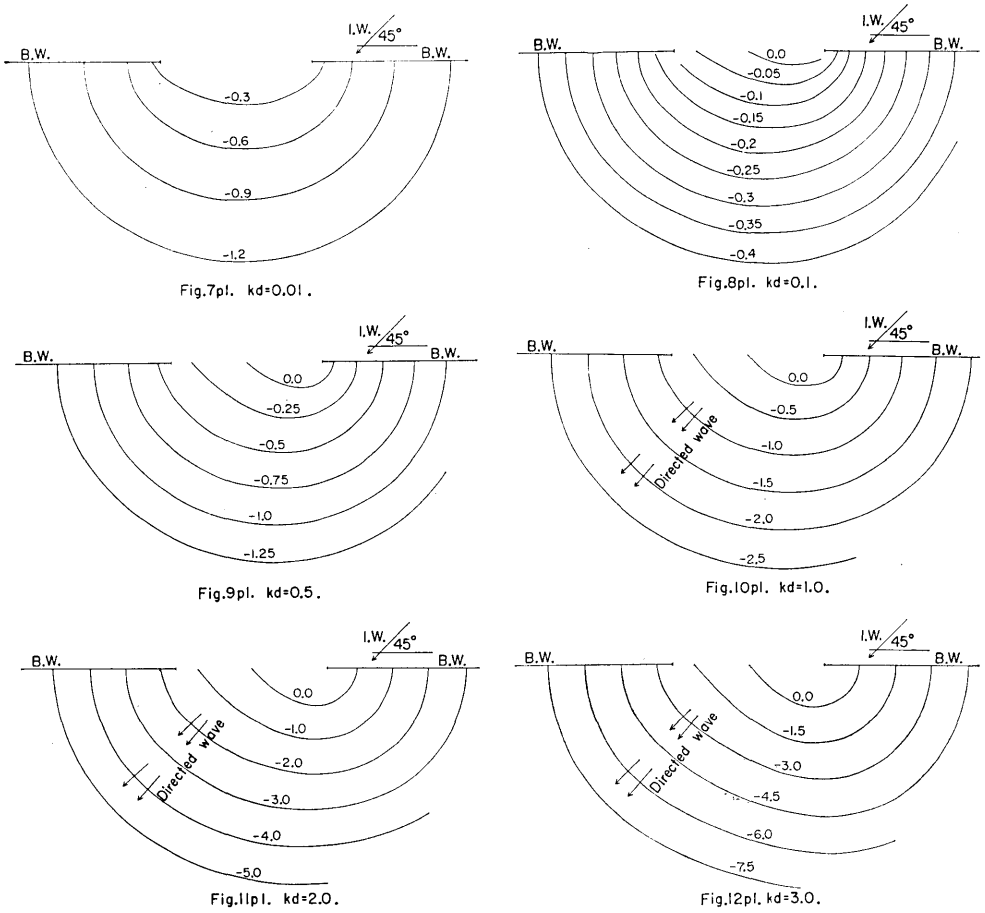

Figs. 7pl–12pl. Phase variation of RST wave in the leeward waters.*

shown, respectively, by the elongation of the contours of the amplitude (see Figs. 9al to 12al) and by the running of the crest lines (see Figs. 10pl to 12pl) toward and normal to the direction of the incident wave travel.

With a view to inquiring into the variation of the reverse current for the incident angle of the incident wave, which has been found in the windward waters around the terminus of the leeward breakwater for small kd, the calculation of the phase of the wave with $kd=0.01$ and 0.04 is made for the incident angle $\theta_{in}=1.8$, 22.5, 45 and 67.5 degrees. The results are given in Figs. 13a (b, c, d) and 14a (b, c, d). According to these figures, the reverse current continues growing with the increase of the incident angle θ_{in} so that the separating point, stated by **S. P.** in the figures, moves away gradually for the increase of θ_{in}.

* See the footnote of Figs. 3-6.

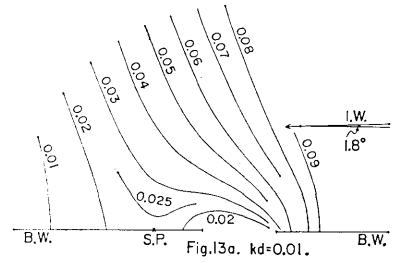

Fig.13a. kd=0.01.

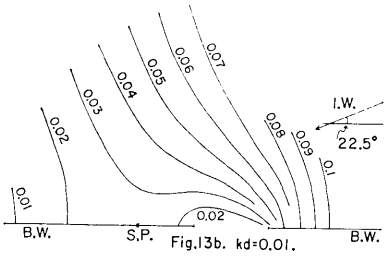

Fig.13b. kd=0.01.

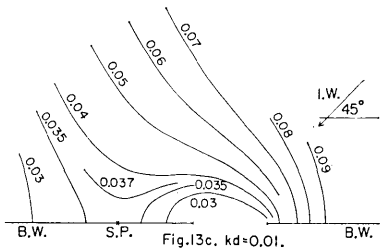

Fig.13c. kd=0.01.

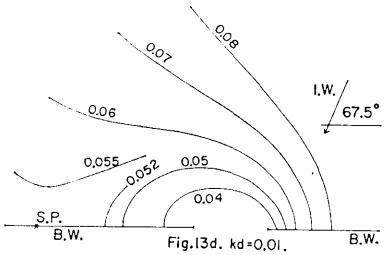

Fig.13d. kd=0.01.

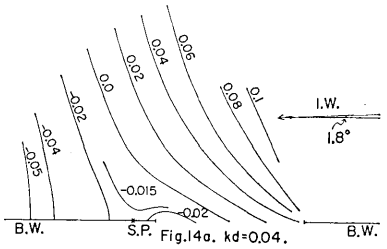

Fig.14a. kd=0.04.

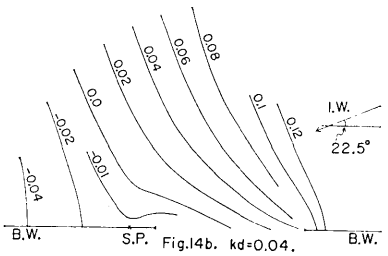

Fig.14b. kd=0.04.

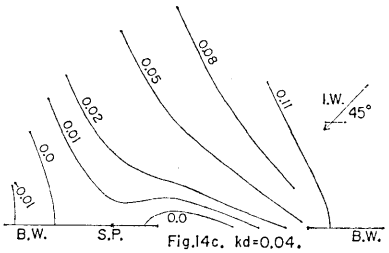

Fig.14c. kd=0.04.

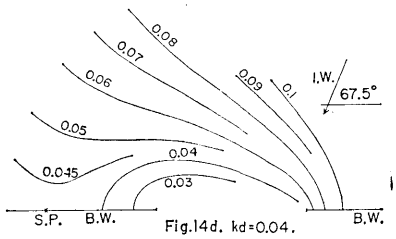

Fig.14d. kd=0.04.

Figs. 13a–14d. Variation of the vererse current for the change of the incident angle of the invading wave.* **S. P.** is the point separating the reverse current from the advancing one.

3,3. RD Wave.

The RD wave is the abbreviation of the reflected and diffracted wave which is exclusive of the incident wave from the RST wave. In other words, the RD wave denote a coastal response for the invasion of the

* See the footnote of Figs. 3–6.

incoming wave. The calculation is based on

$$\bar{\zeta}_{rd}=\bar{\zeta}_{rst}-\zeta_0 \exp(+ik_1x+ik_2y) .$$

ζ_{rd} and ζ_{rst} are the RD and RST waves. The bars denote the conjugate values which refer to the conversion of the incident wave exp $(-i\omega t-ik_1x-ik_2y)$ to exp $(+i\omega t+ik_1x+ik_2y)$. The depiction of the figures of the amplitude and phase is made by $|\bar{\zeta}_{rd}|$ and arg $\bar{\zeta}_{rd}$. The calculated range of kd is 0.01 to 3.0 for the incident angle $\theta_{in}=45$ degrees. The results are shown, respectively, in Figs. 15a (b, c, d) and 16a (b) for the phase and amplitude. The figures relevant to the phase (Figs. 15a, b, c, and d) show that the geometric shadow grows to have a definite boundary line as kd increases from 0.01 to 3.0. According to Figs. 16a

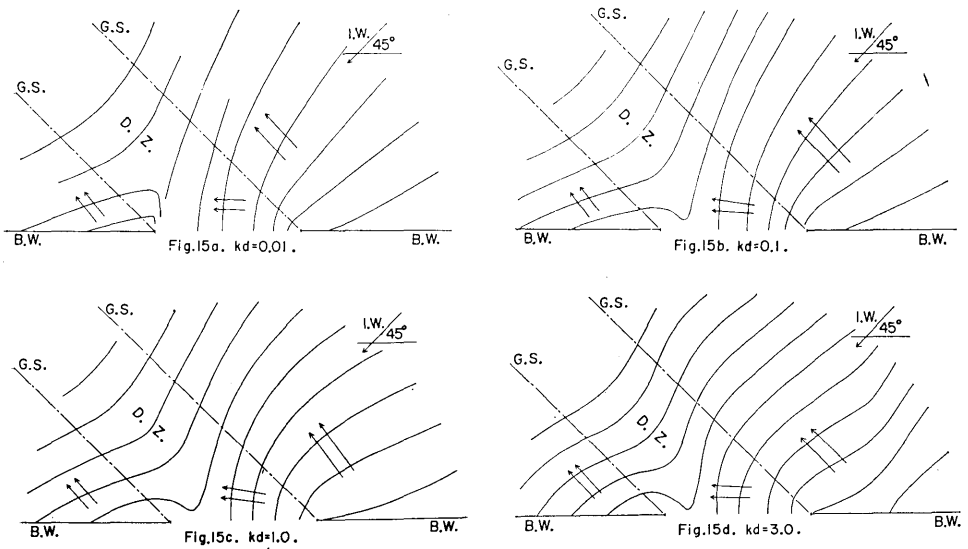

Figs. 15a-d. Phase variation of RD wave in the windward waters.*

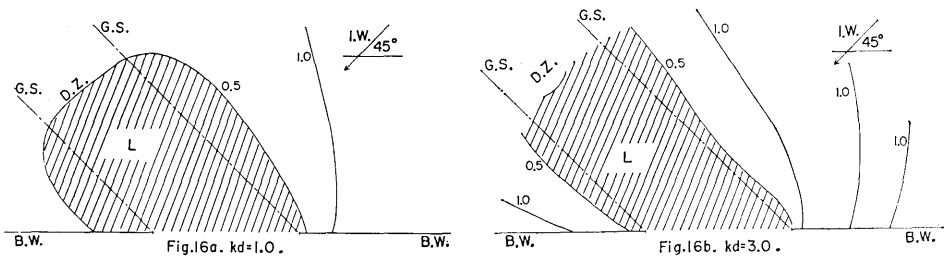

Figs. 16a and b. Amplitude variation of RD wave in the windward waters.* **L** denotes the region of low amplitude.

* For **I. W.** and **B. W.**, the reader should refer to the footnote of Figs. 3-6. **G. S.** and **D. Z.** are the abbreviations of "geometric shadow" and "diffraction zone".

and b, the diffraction zone is characterized by the extension of the low amplitude area (the shaded region in the figures) from the breakwater gap.

3,4. Effect of the Breakwater upon the Diffracted Wave.

The effect of the breakwater wing upon the wave diffracted from the other breakwater is discussed in this section. The method of the analysis is as follows. Let ζ_{right} and ζ_{left} be the wave heights in the models of single right and left breakwaters for the invasion of the incident wave $\exp(+i\omega t+ik_1x+ik_2y)$, which are given by (27). The gross effect of the right-hand (or left-hand) breakwater upon the wave diffracted from the left-hand (or right-hand) breakwater, $\zeta_{e.r.b.}$ (or $\zeta_{e.l.b.}$) is assessed by the equation

$$\zeta_{e.r.b.}\ (\text{or } \zeta_{e.l.b.}) = \bar{\zeta}_{rst} - \zeta_{right}\ (\text{or } \zeta_{left}) \tag{28}$$

where $\bar{\zeta}_{rst}$ is the wave height of the RST wave given in Section *3,2*. The illustration of equation (28) is given in Fig. 17a(b).

The numerical calculation of $\zeta_{e.r.b.}$ (or $\zeta_{e.l.b.}$) is carried out for $kd=$ 0.01, 0.1 and 1.0, the results of which are given in Figs. 18a(b, c), 19a(b, c), 20a(b) and 21a(b).

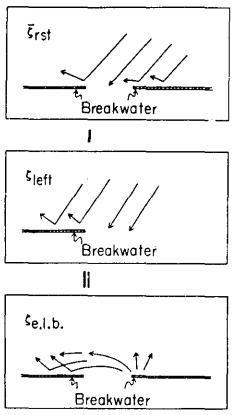

Fig. 17a. Effect of the left-hand breakwater on the wave diffracted from the right-hand one.

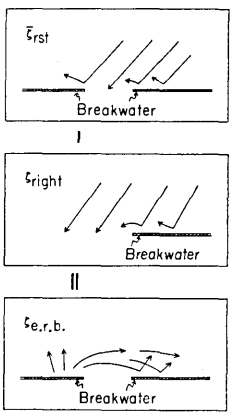

Fig. 17b. Effect of the right-hand breakwater on the wave diffracted from the left-hand one.

Fig. 17a(b). Illustration of equation (28).

Through Figs. 18a(b, c) and 19a(b, c) (the figures of the amplitude relevant to the waves $\zeta_{e.r.b.}$ and $\zeta_{e.l.b.}$ respectively), the regions over 0.1 are shaded. The shadowed area in Figs. 18a, b and c degenerates rapidly with the increase of kd from 0.01 to 1.0, while that in Figs. 19a, b and c occupies nearly the same region through three figures. The reason for this phenomenon is considered to be owing to the incident angle of the incoming wave (θ_{in}) which is, in the present case, 45 degrees against the right-hand breakwater. Through Figs. 18a (b, c) and 19a(b, c), the low-amplitude region is spread out before the breakwater gap which is produced by the reflecting component from the leeward waters. The above low-amplitude region is designated by the letter **L** in the figures.

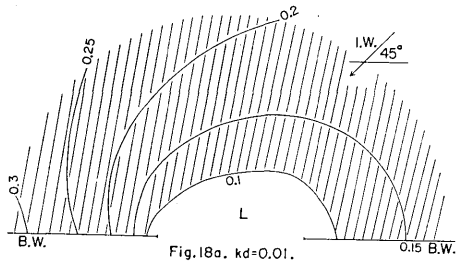

Fig.18a. kd=0.01.

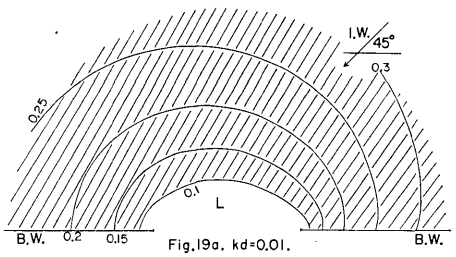

Fig.19a. kd=0.01.

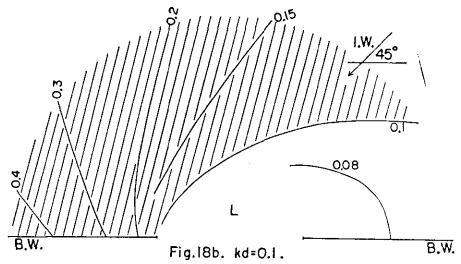

Fig.18b. kd=0.1.

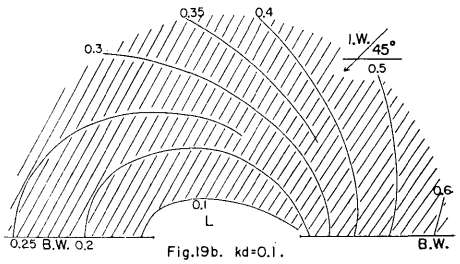

Fig.19b. kd=0.1.

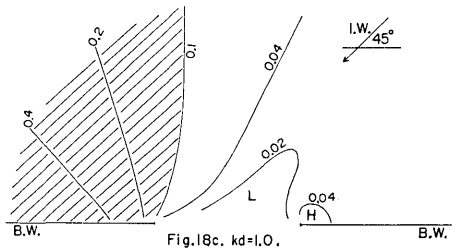

Fig.18c. kd=1.0.

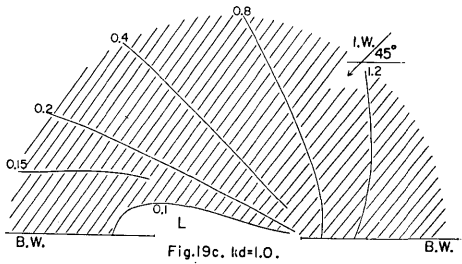

Fig.19c. kd=1.0.

Figs. 18a, b and c. Variation of $|\zeta_{e.r.b.}|$.*

Figs. 19a, b and c. Variation of $|\zeta_{e.l.b.}|$.*

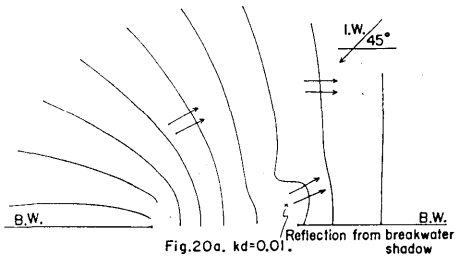

Fig.20a. kd=0.01.

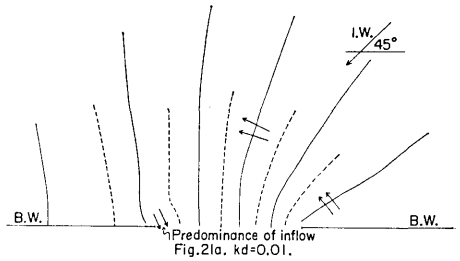

Fig.21a. kd=0.01.

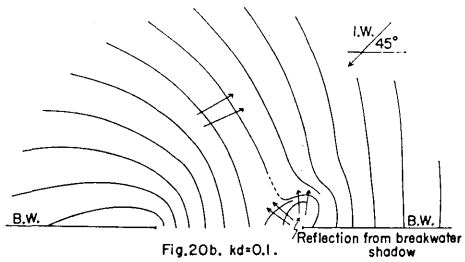

Fig.20b. kd=0.1.

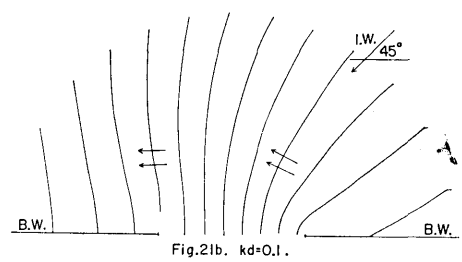

Fig.21b. kd=0.1.

Figs. 20a and b. Variation of arg $\zeta_{e.r.b.}$,*

Figs. 21a and b. Variation of arg $\zeta_{e.l.b.}$.*

* For **I. W.** and **B. W.**, the footnote of Figs. 3-6 should be referred to. The depiction is made only in the windward waters.

As for the phase variation of the diffracted waves (Figs. 20a(b) and 21a(b)), the following facts are found. Comparing Fig. 20a relating to the wave $\zeta_{e.r.b.}$ with Fig. 21a relevant to $\zeta_{e.l.b.}$ for $kd=0.01$, the phase of the former is more retarded than that of the latter. The retardation lessens as kd increases from 0.01 to 0.1 (refer to Figs. 20b and 21b). In Figs. 20a and b, the kinking phase line is found near the terminus of the right-hand breakwater, suggesting the behavior of the reflection of the wave from the breakwater shadow. In Figs. 21a and b, such a behavior is not found. Instead of the above phenomenon, the inflow toward the leeward waters is exposed in Fig. 21a. The arriving wave diffracted from the right-hand breakwater in the case of Fig. 21 is much stronger than that diffracted from the left-hand breakwater in the case of Fig. 20, so that the reflecting behavior from the breakwater shadow in the case of the former is suppressed by the overwhelming inflow toward the leeward waters.

References

Momoi, T., 1967a, 1967b, 1968a, 1968b, 1968c, 1969a and 1969b, A Long Wave around a Breakwater [I], [II], [III], [IV], [V], [VI] and [VII], *Bull. Earthq. Res. Inst.*, **45**, 91-136, **45**, 749-783, **46**, 125-135, **46**, 319-343, **46**, 889-899, **47** 165-184 and **47**, 701-719.

Stoker, J. J., 1957, Water Waves, *Pure and Applied Mathematics, Vol. IV, Interscience Publishers, Inc., New York*, 109-133.

---

40. 防波堤のまわりにおける長波 [VIII]

——斜入射の場合——

地震研究所 桃 井 高 夫

本報告においては防波堤に対して進入波が斜入射する場合（ここで進入波は常に右手の防波堤と鋭角をなすように与えられている）の論議がなされている．数値解析によって判明した著しい現象は次のごとくである．

左手の防波堤端近くの風上側の水域で進入波の進行方向とは逆向きの流れが波長の長い波に対して現われる．そしてこの逆流の規模は進入波の進入角（進入波と右手の防波堤とがなす角）が大きくなるにつれて大きくなってくる．また回析波に対する防波堤端の影響に関する解析において，防波堤の陰から風上側への反射波が見出される．